Journal of Sound and Vibration (2001) **239**(2), 233–254
doi:10.1006/jsvi.2000.3118, available online at http://www.idealibrary.com on IDEAL®

MOVING FORCE IDENTIFICATION: OPTIMAL STATE ESTIMATION APPROACH

S. S. Law

Civil and Structural Engineering Department, The Hong Kong Polytechnic University, Hunghom, Kowloon, Hong Kong, People's Republic of China. E-mail: cesslaw@polyu.edu.hk

AND

Y. L. Fang

Department of Flight Vehicle Design and Applied Mechanics, Beijing University of Aeronautics and Astronautics, Beijing, People's Republic of China

(*Received* 10 *November* 1999, *and in final form* 15 *May* 2000)

Existing techniques to identify moving forces exhibit the common weakness of having large fluctuations in the identified results. A new method of moving force identification is developed in this paper making use of the dynamic programming technique to overcome this weakness. The forces in the state-space formulation of the dynamic system are identified in the time domain using a recursive formula based on several distributed sensor measurements, and responses of the structure are reconstructed using the identified forces for comparison. Like all inverse problems, the computation is ill-conditioned. However, the dynamic programming technique inherently provides bounds to the ill-conditioned forces, and results from the simulation studies and laboratory work show great improvements over existing methods in the accuracy of identification.

1. INTRODUCTION

The vehicle/bridge interaction forces are important for bridge design as they contribute to the live load component in the bridge design code. Direct measurement of the forces using instrumented vehicles is expensive and is subjected to bias [1, 2], while results from computation simulations are subjected to modelling errors [3–5]. Inclusion of the influencing parameters in the model would make it computationally expensive. Systems have been developed for weigh-in-motion of the vehicles [6, 7], but they all measure only the static axle loads. A technique to determine the vehicular loads from the vibration responses of the bridge deck is required such that the different parameters of the bridge and vehicle system are accounted for in the measured responses, and the cost involved would be much less than that by direct measurement.

Some researchers identified forces acting at a fixed location. Whiston [8] and Jordan and Whiston [9] used the arrival-time difference between the maximum and minimum frequency components in the flexural wave in a beam to calculate a preliminary estimation of the force, and a further refinement process is conducted to reconstruct the impact history iteratively so that the force would not have a negative value. Michaels and Pao [10] developed a method that determined an oblique dynamic force using wave motion displacement measurements.

0022-460X/01/020233 + 22 $35.00/0

Other researchers worked on the problem in which both the force history and its location and unknown. Examples include using the modal response data to determine the location of impact forces on the read/write head of computer disks [11]. Doyle [12] also developed a method for determining the location and magnitude of an impact force using the phase difference of the signals measured at two different locations straddling the impact point. Flexural wave propagation response was used to determine the location of the structural impacts.

All the above works are based on the propagating-wave approach which relies on models in the frequency domain. Busby and Trujillo [13] reconstructed the force history using a standing wave approach and Hollandsworth and Busby [14] verified this experimentally with a force applied at a known location and accelerometers were used as sensors. Simonian [15, 16] used a dynamic programming filter to predict wind loads on a structure. Druz *et al.* [17] formulated a non-linear inverse problem and tried to find the location and magnitude of the external force. This force, however, was not general and is confined to a sinusoidal function defined by its amplitude and phase.

Research on the identification of moving forces just started a few years ago. The time domain approach [18] models the structure and forces with a set of second order differential equations. The forces are modelled as step functions in a small time interval. These equations of motion are then expressed in the modal co-ordinates, and they are solved by convolution in time domain. The forces are then identified using the modal superposition principle. The frequency and time domain approach [19] performs Fourier transformation on the equations of motion, which are expressed in modal co-ordinates. The Fourier transforms of the responses are expressed in terms of those for the forces, and the time histories of the forces are found directly by the least-squares method. The modal approach [20] identifies the forces completely in the modal co-ordinates. Measured displacements are converted into modal displacements with an assumed shape function. The modal velocities and accelerations are then obtained by differentiation. The forces are then identified by solving the uncoupled equations of motion in modal co-ordinates.

All the three approaches require the computation of matrix inverse, and they are computationally expensive. These approaches can be shown to be numerically ill-conditioned at the start and end of the time histories.

This paper further explores the area of moving force identification making use of the dynamic programming technique. The forces are identified in the time domain using recursive formula, and responses of the structure are reconstructed using the identified forces for comparison. The forces are identified based on several distributed sensor measurements. Like all inverse problems, the computation is ill-conditioned. However, the dynamic programming technique inherently provides bounds to the ill-conditioned forces, and results from both the simulation studies and laboratory work show great improvements in the accuracy of identification over existing methods. The simulation studies are on the identification of a single force and two forces moving on a simply supported beam. The experiment study has a model car moving on a simply supported beam, and the interaction forces are identified from velocity and bending moment responses of the beam.

2. ASSUMPTIONS

The following assumptions are made on the dynamic system model:

1. The changes in the system characteristics, i.e., the stiffness, damping and mass matrices under the passage of the force are negligible.

2. Structural damping is included in the analysis.
3. The structure may not be at rest before the application of the load.
4. There is no restriction on the type of force history to be identified.
5. The Euler–Bernoulli beam model is used with the shear effect neglected.

3. NODAL FORCES FROM AN APPLIED FORCE

When a force time history f_1 is applied on a two-dimensional finite beam element of length l between the ith and $(i+1)$th nodes at a point distance x from the left end, the nodal forces at each end of the beam element can be represented by

$$R_i = \left(1 - \frac{3x^2}{l^2} + 2\frac{x^3}{l^3}\right) f_1,$$

$$M_i = \left(x - \frac{2x^2}{l} + \frac{x^3}{l^2}\right) f_1,$$

$$R_{i+1} = \left(\frac{3x^2}{l^2} - \frac{2x^3}{l^3}\right) f_1,$$

$$M_{i+1} = \left(\frac{x^3}{l^2} - \frac{x^2}{l}\right) f_1, \tag{1}$$

where R_i, R_{i+1} are the vertical nodal forces, and M_i, M_{i+1} are the nodal bending moments at the ith and $(i+1)$th node of the structure respectively. These nodal forces are grouped into the global force vector as

$$\mathbf{P} = \mathbf{Y}(\mathbf{x}) \cdot f_1, \tag{2}$$

where $\mathbf{P}$ is the nodal force vector and $\mathbf{Y}(x)$ is the vector on the location of the applied force. For the case of multi-forces acting on the beam element, the global force vector arising from the ith force is represented by

$$\mathbf{P}_i = \mathbf{Y}(x_i) \cdot f_i. \tag{3}$$

4. STATE-SPACE MODEL FORMULATION

The finite element representation of an n-d.o.f.s dynamic system is given by

$$\mathbf{M}\ddot{\mathbf{u}} + \mathbf{C}\mathbf{u} + \mathbf{K}\mathbf{u} = \mathbf{P}, \tag{4}$$

where $\mathbf{u}$ is a vector containing all the displacements of the model, $\dot{u}$ is the first derivative of $\mathbf{u}$ with respect to time t, $\mathbf{M}$ is the system mass matrix, $\mathbf{C}$ is the system damping matrix, $\mathbf{K}$ is the system stiffness matrix, and $\mathbf{P}$ represents the system of exciting forces which is a function of the location and magnitude of the applied forces as shown in equation (3).

Using the state-space formulation, equation (4) is converted into a set of first order differential equations as follows:

$$\dot{\mathbf{X}} = \mathbf{K}^*\mathbf{X} + \bar{\mathbf{P}}, \tag{5}$$

where

$$\mathbf{X} = \begin{bmatrix} \mathbf{u} \\ \dot{\mathbf{u}} \end{bmatrix}_{2n\times 1}, \quad \mathbf{K}^* = \begin{bmatrix} 0 & \mathbf{I} \\ -M^{-1}\mathbf{K} & -M^{-1}\mathbf{C} \end{bmatrix}_{2n\times 2\pi},$$

$$\bar{\mathbf{P}} = \begin{bmatrix} \mathbf{0} \\ -\mathbf{M}^{-1}\mathbf{P} \end{bmatrix}_{2n\times 1}$$

$$= \begin{bmatrix} 0 \\ -\mathbf{M}^{-1}\mathbf{Y} \end{bmatrix}_{n\times n_f} \mathbf{f}_{nf\times 1}, \tag{6}$$

where $\mathbf{X}$ represents a vector of state variables of length $2n$ containing the displacements and velocities of the nodes, n_f is the number of forces, and $\mathbf{f}$ is a vector of length n_f representing the unknown applied forces. These differential equations are then rewritten as discrete equations using the standard exponential matrix representation.

$$\mathbf{X}_{j+1} = \mathbf{F}\mathbf{X}_j + \bar{\mathbf{G}}_{j+1}\bar{\mathbf{P}}_j, \tag{7}$$

$$\mathbf{F} = \mathbf{e}^{K^*h} \tag{8}$$

and

$$\bar{\mathbf{G}} = \mathbf{K}^{*-1}(\mathbf{F} - \mathbf{I}), \tag{9}$$

where matrix $\mathbf{F}$ is the exponential matrix, and together with matrix $\bar{\mathbf{G}}$ it represents the dynamics of the system, $(j+1)$ denotes the value at the $(j+1)$th time step of computation, the time step h represents the time difference between the variable states $\mathbf{X}_j$ and $\mathbf{X}_{j+1}$ in the computation, and $\bar{\mathbf{G}}$ is a matrix relating the forces to the system. Substituting equations (6) and (9) into equation (7) we have

$$\mathbf{X}_{j+1} = \mathbf{F}\mathbf{X}_j + \mathbf{G}_{j+1}\,\mathbf{f}_j, \tag{10}$$

where

$$\mathbf{G} = \bar{\mathbf{G}}_{2n\times 2n}\begin{bmatrix} 0 \\ -\mathbf{M}^{-l}\mathbf{Y} \end{bmatrix}_{2n\times nf}. \tag{11}$$

5. PROBLEM STATEMENT

The problem we have is one in which the system matrices $\mathbf{K}$, $\mathbf{C}$ and $\mathbf{M}$ are known together with information on some of the displacements and velocities. However, the forcing term f is unknown. The goal of this problem is to find the forcing term $\mathbf{f}$ that causes the system described in equation (10) to best match the measurement.

In practice, it is not possible to measure all the displacements and velocities, and, only certain combinations of the variables $\mathbf{X}_j$ are measured. The measurement equation is given as

$$\mathbf{d}_j = \mathbf{Q}\mathbf{X}_j, \tag{12}$$

where $\mathbf{d}_j$ is an $(m\times 1)$ measurement vector, $\mathbf{Q}$ is an $(m\times 2n)$ selection matrix relating the measurements to the state variables, and $\mathbf{X}_j$ is of dimension $(2n\times 1)$. The actual

measurements are represented by a vector $\mathbf{Z}_j$ which is of the same dimension as $\mathbf{d}_j$. The number of measured variables m is usually much less than the number of state variables (or n d.o.f.s of the system) but greater than or equal to n_f, the length of vector $\mathbf{f}$. In the case of a two-dimensional simply supported beam divided into L elements, $n = 2(L + 1) - 2$ including all vertical displacements and rotational displacements at each of its nodes.

When the unknown force $\mathbf{f}_j$ is included in equation (10), an exact match of the model with the measured data is usually not possible. This is due to the fact that all measurements have some degree of noise. Even the least-squares criterion is not sufficient because a mathematical solution that will minimize the least-squares error E represented by

$$\mathbf{E} = \sum_{j=I}^{N} ((\mathbf{Z}_j - \mathbf{QX}_j), \mathbf{A}(\mathbf{Z}_j - \mathbf{QX}_j)) \tag{13}$$

will usually end up with the model exactly matching the data. (x, y) in equation (13) denotes the inner product of two vectors x and y. This situation could be avoided by adding a smoothing term to the least-squares error [21, 22] to become a non-linear least-squares problem

$$\mathbf{E} = \sum_{j=1}^{N} ((\mathbf{Z}_j - \mathbf{QX}_j), \mathbf{A}(\mathbf{Z}_j - \mathbf{QX}_j) + (\mathbf{f}_j, \mathbf{Bf}_j)). \tag{14}$$

The second term is known as the regularization parameter and the method is called the Tikhonov [23] method. Matrices $\mathbf{A}(m \times m)$ and $\mathbf{B}(n_f \times n_f)$ are symmetric positive-definite weighting matrices that provide the flexibility of weighting the measurements and the forcing terms. Matrix $\mathbf{A}$ is usually an identity matrix and matrix $\mathbf{B}$ is a diagonal matrix. The second term with the positive parameter $\mathbf{B}$ has the effect of smoothing the identified forces. A small value of $\mathbf{B}$ causes the solution to match the data closely but produces large oscillatory deviations. A large value of $\mathbf{B}$ produces smooth forces that may not match the data well. When $\mathbf{B}$ is zero, the solution becomes that for the least-squares problem.

6. STRAIN MEASUREMENTS

For a two-dimensional finite beam element of length l represented by the degrees of freedom $(u_1, \theta_1, u_2, \theta_2)$ at its two ends, the strain at any cross-section distance x from the left end of the beam element can be given in terms of the d.o.f.s. at its two ends as

$$\varepsilon_x = \left(\frac{-y}{l^3}\right)(12x - 6l)u_1 - l(6x - 4l)\theta_1 - (12x - 6l)u_2 + l(6x - 2l)\theta_2], \tag{15}$$

where y represents the distance from the neutral axis of the beam. In the verification of this study, the strain measurements and hence the bending moments are related to all of the transverse displacements and rotational displacements at the ends of the element using this relationship.

7. MATRIX G FOR TWO MOVING FORCES WITH KNOWN SPEED

Suppose that we have two forces spaced at a constant distance moving across a simply supported beam at a constant speed c. The matrices $\bar{\mathbf{G}}$ and $\mathbf{G}$ in equations (9) and (11),

respectively, vary for different locations of the forces. Rewrite equations (2) and (9) as

$$\mathbf{P} = [\mathbf{Y}(\mathbf{x}_1), \mathbf{Y}(x_2)] \begin{pmatrix} \mathbf{f}_1 \\ \mathbf{f}_2 \end{pmatrix}, \tag{16}$$

$$\bar{\mathbf{G}} = \begin{bmatrix} \bar{\mathbf{G}}_{11} & \bar{\mathbf{G}}_{12} \\ \bar{\mathbf{G}}_{21} & \bar{\mathbf{G}}_{22} \end{bmatrix} \tag{17}$$

and equation (6) becomes

$$\bar{\mathbf{P}} = \begin{bmatrix} 0 & 0 \\ -\mathbf{M}^{-1}\mathbf{Y}(\mathbf{x}_1) & -\mathbf{M}^{-1}\mathbf{Y}(x_2) \end{bmatrix} \begin{pmatrix} \mathbf{f}_1 \\ \mathbf{f}_2 \end{pmatrix}. \tag{18}$$

The discrete representation of the system in equation (7) can then be written as

$$\begin{aligned} \mathbf{X}_{j+1} &= \mathbf{F}\mathbf{X}_j + \bar{\mathbf{G}}_{j+1}\bar{\mathbf{P}}_j \\ &= \mathbf{F}\mathbf{X}_j + \begin{bmatrix} \bar{\mathbf{G}}_{11} & \bar{\mathbf{G}}_{12} \\ \bar{\mathbf{G}}_{21} & \bar{\mathbf{G}}_{22} \end{bmatrix} \begin{bmatrix} 0 & 0 \\ -\mathbf{M}^{-1}\mathbf{Y}(\mathbf{x}_1) & -\mathbf{M}^{-1}\mathbf{Y}(\mathbf{x}_2) \end{bmatrix} \begin{pmatrix} \mathbf{f}_1 \\ \mathbf{f}_2 \end{pmatrix} \\ &= \mathbf{F}\mathbf{X}_j + \begin{bmatrix} -\bar{\mathbf{G}}_{12}\mathbf{M}^{-1}\mathbf{Y}(\mathbf{x}_1) & -\bar{\mathbf{G}}_{12}\mathbf{M}^{-1}\mathbf{Y}(\mathbf{x}_2) \\ -\bar{\mathbf{G}}_{22}\mathbf{M}^{-1}\mathbf{Y}(\mathbf{x}_1) & -\bar{\mathbf{G}}_{22}\mathbf{M}^{-1}\mathbf{Y}(\mathbf{x}_2) \end{bmatrix} \begin{pmatrix} \mathbf{f}_1 \\ \mathbf{f}_2 \end{pmatrix} \\ &= \mathbf{F}\mathbf{X}_j + \mathbf{G}_{j+1}(\mathbf{x}_1, \mathbf{x}_2) \begin{pmatrix} \mathbf{f}_1 \\ \mathbf{f}_2 \end{pmatrix} \end{aligned} \tag{19}$$

and in matrix form as

$$\mathbf{X}_{j+1} = \mathbf{F}\mathbf{X}_j + \mathbf{G}_{j+1}\mathbf{f}_j, \tag{20}$$

where G_{j+1} is the value at the $(j+1)$th time step. Note the equation (20) is the same as equation (10) but for two moving forces.

8. DYNAMIC PROGRAMMING

To minimize the least-squares error E in equation (14) over the sequence of the forcing vector $\mathbf{f}_j$, the dynamic programming method [24] and Bellman's Principle of Optimality [25] are applied. The minimum value of E at the nth stage for any initial state $\mathbf{X}$ is written as

$$\mathbf{g}_n(\mathbf{X}) = \min_{\mathbf{f}_j} E_n(\mathbf{X}, \mathbf{f}_j). \tag{21}$$

A recursive formula for equation (21) is derived from Bellman's Principle of Optimality as

$$\mathbf{g}_{n-1}(\mathbf{X}) = \min_{f_{n-1}} ((\mathbf{Z}_{n-1} - \mathbf{Q}\mathbf{X}), \mathbf{A}(\mathbf{Z}_{n-1} - \mathbf{Q}\mathbf{X}) + (\mathbf{f}_{n-1}, \mathbf{B}\mathbf{f}_{n-1}) + \mathbf{g}_n(\mathbf{F}\mathbf{X} + \mathbf{G}_n\mathbf{f}_{n-1})). \tag{22}$$

This equation represents the classic dynamic programming structure in that the minimum at any point is determined by selecting the decision f_{n-1} to minimize the immediate cost (the first and second terms) and the remaining cost resulting from the decision (the third term). It is noted that the minimization is performed over a previously determined function g_n. The

terms f_n and g_n are the optimal forcing term and the optimal cost term respectively. The solution is obtained by starting at the end of the process, $n = N$, and working backward to $n = 1$. At the endpoint, the minimum is determined from

$$g_N(\mathbf{X}) = \min_{f_N} [(\mathbf{Z}_N - \mathbf{QX}), \mathbf{A}(\mathbf{Z}_N - \mathbf{QX}) + \mathbf{f}_N, \mathbf{Bf}_N]. \tag{23}$$

With $f_N = 0$, we obtain the minimum solution as shown in equation (24) by expanding equation (23)

$$\mathbf{g}_N(\mathbf{X}) = \mathbf{q}_N + (\mathbf{X}, \mathbf{S}_N) + (\mathbf{X}, \mathbf{R}_N\mathbf{X}), \tag{24}$$

where

$$\begin{aligned} \mathbf{q}_N &= \mathbf{Z}_N, \mathbf{AZ}_N, \\ \mathbf{S}_N &= -2\mathbf{Q}_N^{\mathrm{T}}\mathbf{AZ}_N, \\ \mathbf{R}_N &= \mathbf{Q}_N^{\mathrm{T}}\mathbf{AQ}_N. \end{aligned} \tag{25}$$

These are the initial conditions for working backward at $n = N$. Substituting equation (24) for the nth and $(n-1)$th steps into equation (22), and expanding the right-hand side of the equation, we have

$$\mathbf{q}_{n-1} + (\mathbf{X}, \mathbf{S}_{n-1}) + (\mathbf{X}, \mathbf{R}_{n-1}\mathbf{X}) = \min_{f_{n-1}} [(f_{n-1} + V_n\mathbf{X} + \mathbf{U}_n), \mathbf{H}_n(\mathbf{f}_{n-1} + \mathbf{V}_n\mathbf{X} + \mathbf{U}_n) + \mathbf{r}_{n-1}(\mathbf{X})], \tag{26}$$

where

$$\mathbf{H}_n = \mathbf{B} + \mathbf{G}_n^{\mathrm{T}}\mathbf{R}_n\mathbf{G}_n, \quad 2\mathbf{H}_n\mathbf{V}_n = 2\mathbf{G}_n^{\mathrm{T}}\mathbf{R}_n\mathbf{F}, \quad \mathbf{V}_n = \mathbf{H}_n^{-1}\mathbf{G}_n^{\mathrm{T}}\mathbf{R}_n\mathbf{F},$$

$$2\mathbf{H}_n\mathbf{U}_n = \mathbf{G}_n^{\mathrm{T}}\mathbf{S}_n, \quad \mathbf{U}_n = (\mathbf{H}_n^{-1}\mathbf{G}_n^{\mathrm{T}}\mathbf{S}_n)/2.$$

$$\mathbf{r}_{n-1}(\mathbf{X}) = \begin{bmatrix} (\mathbf{q}_n + \mathbf{Z}_{n-1}^{\mathrm{T}}\mathbf{AZ}_{n-1}) + \mathbf{X}^{\mathrm{T}}(\mathbf{Q}^{\mathrm{T}}\mathbf{AQ} + \mathbf{F}^{\mathrm{T}}\mathbf{R}_n\mathbf{F})\mathbf{X} + \mathbf{X}^{\mathrm{T}}(\mathbf{F}^{\mathrm{T}}\mathbf{S}_n - 2\mathbf{Q}^{\mathrm{T}}\mathbf{AZ}_{n-1}) \\ -X^{\mathrm{T}}\mathbf{V}_n^{\mathrm{T}}\mathbf{H}_n\mathbf{V}_n\mathbf{X} - \mathbf{U}_n^{\mathrm{T}}\mathbf{H}_n\mathbf{U}_n - 2\mathbf{X}^{\mathrm{T}}\mathbf{V}_n^{\mathrm{T}}\mathbf{H}_n\mathbf{U}_n \end{bmatrix}.$$

Minimizing the term on the right-hand side of equation (26) yields the optimal forcing term as

$$\mathbf{f}_{n-1} = -\mathbf{H}_n^{-1}\mathbf{G}_n^{\mathrm{T}}\left[\mathbf{R}_n\mathbf{FX}_{n-1} + \frac{\mathbf{S}_n}{2}\right] \tag{27}$$

and equation (26) becomes

$$\mathbf{q}_{n-1} + (\mathbf{X}, S_{n-1}) + (\mathbf{X}, \mathbf{R}_{n-1}\mathbf{X}) = \mathbf{r}_{n-1}(\mathbf{X}). \tag{28}$$

Equating like powers of $\mathbf{X}$ in equation (28) will yield the following relationship:

$$\begin{aligned} \mathbf{R}_{n-1} &= \mathbf{Q}^{\mathrm{T}}\mathbf{AQ} + \mathbf{F}^{\mathrm{T}}[\mathbf{I} - \mathbf{R}_n^{\mathrm{T}}\mathbf{G}_n\mathbf{H}_n^{-1}\mathbf{G}_n^{\mathrm{T}}]\mathbf{R}_n\mathbf{F}, \\ \mathbf{S}_{n-1} &= -2\mathbf{Q}^{\mathrm{T}}\mathbf{AZ}_{n-1} + \mathbf{F}^{\mathrm{T}}[\mathbf{I} - \mathbf{R}_n^{\mathrm{T}}\mathbf{G}_n\mathbf{H}_n^{-1}\mathbf{G}_n^{\mathrm{T}}]\mathbf{S}_n. \end{aligned} \tag{29}$$

These are the recursive formulae required to determine the optimal solution of equation (22). The complete sequence of operations is as follows:

Step 1: Matrices **Q** and **Z** and the speed of the forces are obtained from measurement;
Step 2: Matrix $\bar{\mathbf{G}}$ and hence matrix **G** are obtained from information on the location of the forces from equations (9) and (19);
Step 3: Compute the initial values $\mathbf{q}_N$, $\mathbf{R}_N$ and $\mathbf{S}_N$ from equation (25); compute $\mathbf{H}_N$ from equation (26);
Step 4: Compute $\mathbf{S}_{n-1}$ and $\mathbf{R}_{n-1}$ from equation (29) for $n = N$ to 1;
Step 5: Initial condition of **X** is set as zero and compute the responses $\mathbf{X}_{j+1}$ from equation (20) for $j = 0$ to N, and compute the forces $\mathbf{f}_{n-1}$ from equation (27) for $n = 1$ to N;
Step 6: Steps 1–5 are repeated for a different smoothing parameter **B**. Convergence is reached when the error computed from equation (30) is reduced to a predetermined value.

9. SIMULATION AND RESULTS

The proposed method is studied for its accuracy and effectiveness in identifying the following simulated forces

(a) for single moving force identification

$$f_1(t) = 40\,000\,[1 + 0{\cdot}1\sin(10\pi t) + 0{\cdot}05\sin(40\pi t)]\ \mathrm{N};$$

(b) for two moving forces identification

$$f_1(t) = 20\,000\,[1 + 0{\cdot}1\sin(10\pi t) + 0{\cdot}05\sin(40\pi t)]\ \mathrm{N},$$

$$f_2(t) = 20\,000\,[1 - 0{\cdot}1\sin(10\pi \mathrm{t}) + 0{\cdot}05\sin(50\pi t)]\ \mathrm{N}.$$

The two forces are at a constant spacing of 4 m apart and they are moving together on a simply supported beam at a velocity of 40 m/s. The physical parameters of the beam are:

$$EI = 1{\cdot}274916 * 10^{11}\,\mathrm{N\,m^2}, \qquad \rho A = 12\,000\ \mathrm{kg/m}, \qquad L = 40\ \mathrm{m}.$$

The lowest three natural frequencies of the beam are 3·2, 12·8 and 28·8 Hz. The finite element model of the beam consists of 10 elements with 11 nodes and 20 rotational and translational d.o.f.s. The state variable matrix **X** has a dimension of (40×1). A sampling frequency of 200 Hz is used indicating that 100 Hz is the upper frequency limit of the study. The time when there are forces on the beam is 1·1 s, and 220 data points are used.

Dynamic analysis was performed on this system to find the velocity and bending moment time histories at specified locations. Five per cent root-mean-square normally distributed random noise with zero mean and unit standard deviation was added to these responses to simulate the polluted measurements.

The error in the force identification is calculated by the following equation where $\|\bullet\|$ is the norm of a matrix:

$$Error = \frac{\|\mathbf{f}_{identified} - \mathbf{f}_{true}\|}{\|\mathbf{f}_{true}\|} \times 100\%. \tag{30}$$

Since the true force is known, the optimal regularization parameter **B** is obtained by comparing the true force $\mathbf{f}_{true}$ with the identified values $\mathbf{f}_{identified}$, and an error curve can be

TABLE 1

Error in one force identification (*in per cent*) (*with* 5% *noise in response*)

Sensor location and response type	Moment	Velocity	Both
1/2 span	26·8	24·5	26·9
1/4 span	26·1	21·7	26·0
1/2 span, 1/4 span	26·7	19·8	26·6

plotted for different values of **B**. The error is calculated from equation (30). It is noted that the optimal value of **B** corresponds to the smallest error.

If both the measured bending moments and velocities are used together to identify the moving forces, the velocity component and the bending moment component in the vector **X** in equation (10) should be scaled by their respective norms to have dimensionless units.

9.1. SINGLE-FORCE IDENTIFICATION

Nine combinations of the responses at 1/4 and 1/2 span as shown in Table 1 are used in the identification. The errors in Table 1 show that the use of single or multiple responses does not cause significant difference in the errors of identification. Results not shown here indicate that the use of an additional sensor at 3/4 span does not improve significantly the identified results.

The time histories and the PSDs of the calculated and true forces for cases of (1/4v, 1/2v) and (1/4m, 1/4v) are shown in Figure 1. The time histories closely match each other except at the start and end of the time duration. It is found that the variation in the identified forces increases with decrease in **B**. An inspection of the PSDs of the force reveals that good matching between the forces is found around the exciting frequencies but with large noise in the upper frequency range. The random noise in the polluted responses is reflected in the upper frequency range of the identified forces with little adverse effect on the results in the lower frequency range. The use of bending moments seems to cause poorer performances compared with the velocities.

The reconstructed bending moment and velocity at 1/4 span are compared with the measured ones in Figures 2 and 3. The time histories match closely with the true ones. The PSDs of the responses indicate that errors exist in the upper frequency range which is again suspected to be due to the simulated noise effect.

9.2. TWO-FORCES IDENTIFICATION

Bending moment and/or velocity responses at 1/4, 1/2 and 3/4 spans in 20 combinations as shown in Table 2 are used to identify the two forces. The results are obtained in a manner similar to the single-force identification.

The errors between the calculated and the true forces are shown in Table 2 for different sensor combinations. The errors calculated by the time domain method (TDM) [18] are also included in brackets for comparison. Note that the TDM uses acceleration measurements instead of velocity measurements in the identification. The proposed method in general gives far smaller error than the time domain method. It is only in the case of using

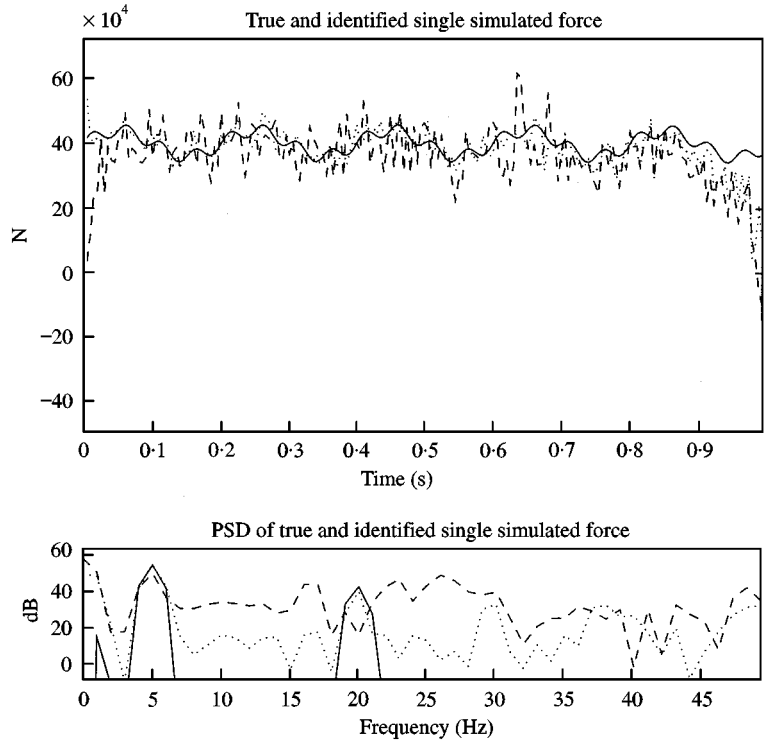

Figure 1. Identified single force and power spectrum from simulation: ——, true; ·····, 1/4v, 1/2v; – – –, 1/4m, 1/4v.

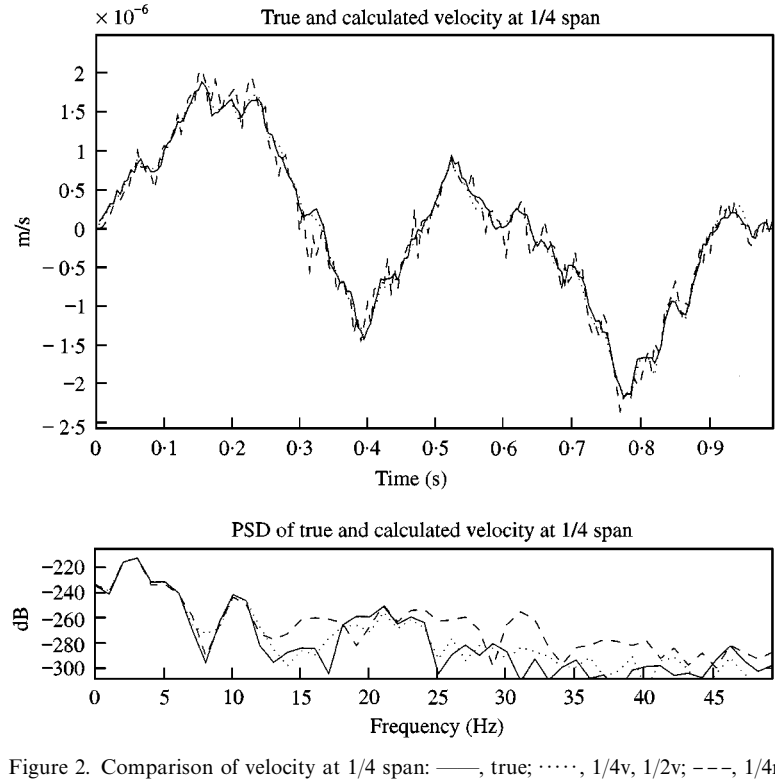

Figure 2. Comparison of velocity at 1/4 span: ——, true; ·····, 1/4v, 1/2v; – – –, 1/4m, 1/4v.

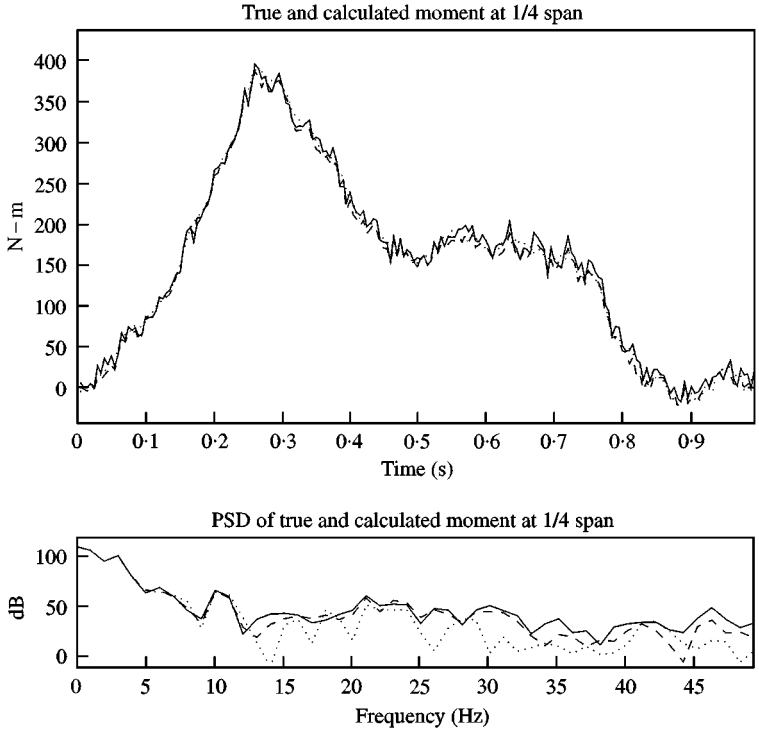

Figure 3. Comparison of bending moment at 1/4 span: ——, true; ·····, 1/4v, 1/2v; – – –, 1/4m, 1/4v.

TABLE 2

Error in two-forces identification (*in per cent*) (*with* 5% *noise in response*)

Sensor location and response type	First force	Second force	Total force
1/4m, 1/2m	35·6†	37·4†	24·3
1/4v, 1/2v	47·5(222)	48·7(78·6)	33·5
1/2m, 1/2v	36·3†	38·4†	24·5
1/4m 1/4v	38·7†	40·6†	27·3
1/2m, 1/4v	36·4†	38·4†	24·1
1/4m, 1/2m, 3/4m	32·1†	33·1†	20·6
1/4v, 1/2v, 3/4v	38·9(10·7)	39·8(10·7)	27·5
1/4m, 1/2m, 1/4v	35·6†	37·4†	24·3
1/2m, 3/4m, 1/4v	33·5	34·1	21·5
1/2v, 3/4m, 3/4v	35·5	37·7	25·8
1/4m, 1/2m, 1/2v	35·6†	37·4(474)	24·3
1/4m, 1/4v, 1/2v	38·7(206)	40·6(156)	27·3
1/2m, 1/4v, 1/2v	36·3(193)	38·4(46·8)	24·5
1/2m, 1/4v, 3/4v	36·4	38·4	24·1
1/4m, 1/2m, 1/4v, 1/2v	35·6(201)	37·4(49·7)	24·0
1/4m, 1/2m, 1/2v, 3/4v	32·1	33·2	20·7
1/2m, 1/4v, 1/2v, 3/4v	36·4	38·4	24·1
1/4m, 1/2m, 3/4m, 1/4v, 1/2v	32·1	33·2	20·7
1/4m, 1/2m, 1/4v, 1/2v, 3/4v	35·6	37·3	24·0
1/4m, 1/2m, 3/4m, 1/4v, 1/2v, 3/4v	32·1	33·1	20·6

†Indicates error larger than 1000%.

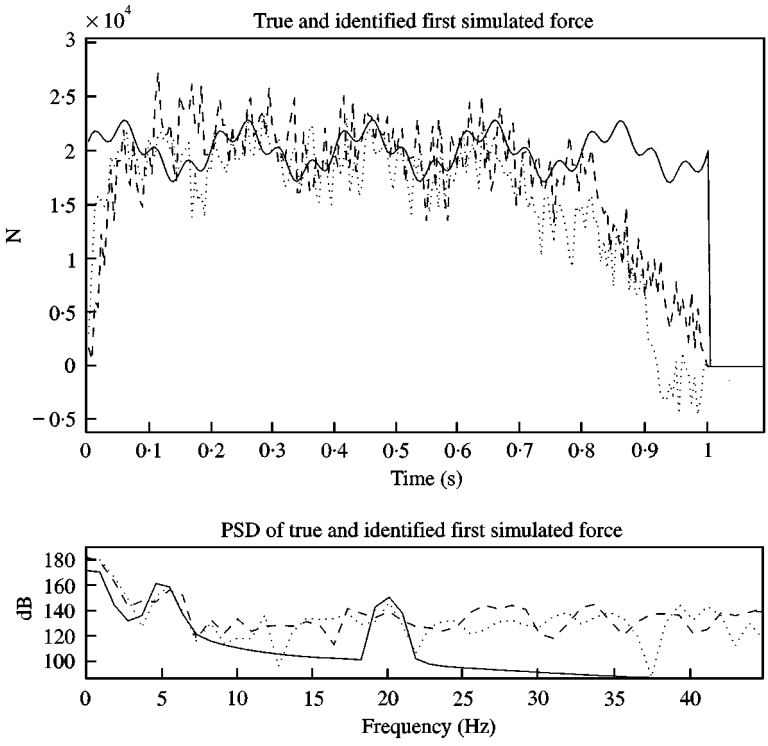

Figure 4. Identified first force and power spectrum from simulation: ——, true; · · · · ·, 1/4v, 1/2v, 3/4v; – – –, 1/4m, 1/2m, 3/4m.

three acceleration measurements that the TDM gives better results than the present case using three velocities. The results shown in Table 2 indicate that (1) many sensor combinations would give similar errors in the identified forces; (2) the use of more than two sensors may not improve the result; and (3) both velocity and bending moment give approximately the same accuracy in the identified forces.

The time histories and PSDs of the identified forces from using (1/4v, 1/2v, 3/4v) and (1/4m, 1/2m, 3/4m) sensor combinations are shown in Figures 4–6. All the identified forces vary closely with the true force in the middle length of the time duration between 0·25 and 0·75 s. The results have a lot of variations due to the simulated noise effect. Other results not shown here using different sensor combinations also exhibit a similar pattern in the identified forces. Note that the discrepancies at the start and end of the time histories contribute greatly to the overall error.

The above results show that accuracy in two-forces identification is lower than that in single-force identification. This is due to a component in the simulated individual forces with same amplitude and opposite phase. This results in large errors in the time histories. The combined force shown in Figure 6 indicates that most of these errors are cancelled out leading to a greatly improved time history and reduced error in the combined identified force as shown in Table 2.

10. EXPERIMENT AND RESULTS

The experimental set-up is shown diagrammatically in Figure 7. The main beam 3376 mm long with 100 mm × 25 mm uniform cross-section is simply supported.

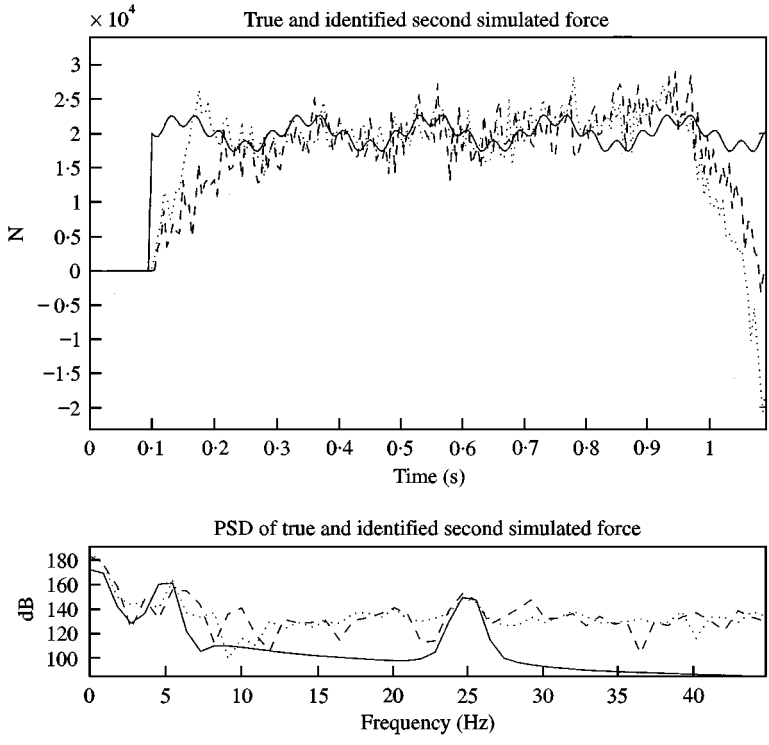

Figure 5. Identified second force and power spectrum from simulation: ——, true; ·····, 1/4v, 1/2v, 3/4v; – – –, 1/4m, 1/2m, 3/4m.

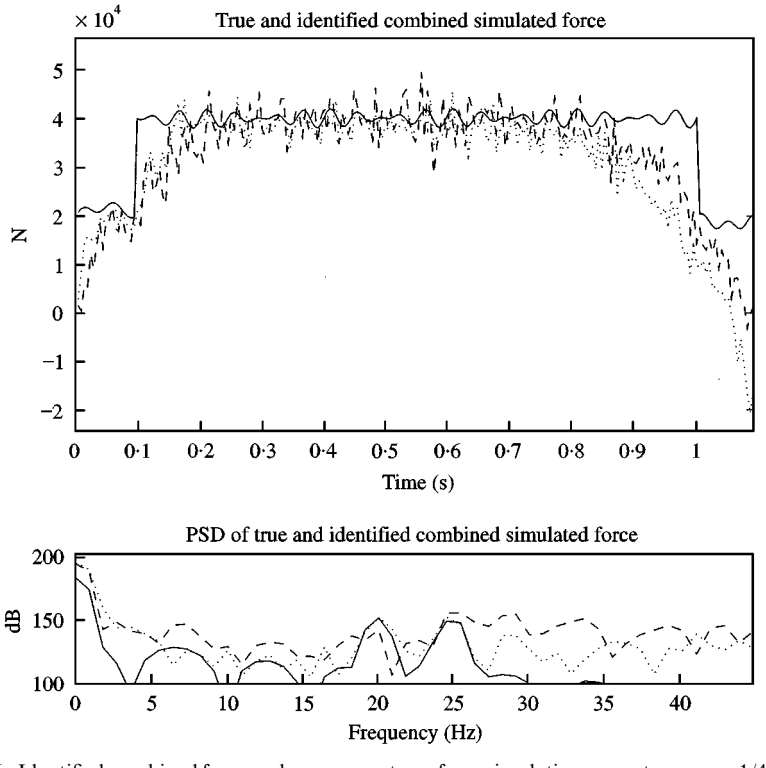

Figure 6. Identified combined force and power spectrum from simulation: ——, true; ·····, 1/4v, 1/2v, 3/4v; – – –, 1/4m, 1/2m, 3/4m.

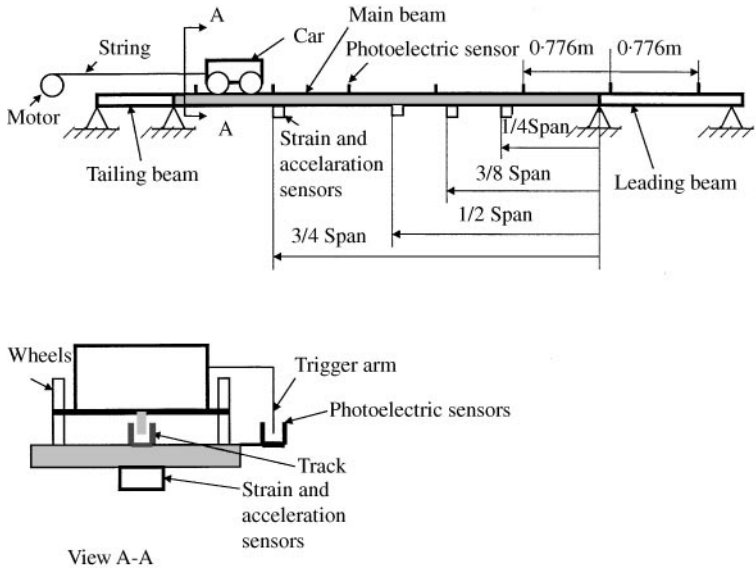

Figure 7. Diagramatic drawing of experimental set-up.

A U-shaped aluminium section on the upper surface of the beams served as direction guide for the car. An electric motor is used to pull a model car along the guide with a string wound on the shaft of the motor. The rotating speed of the motor can be adjusted for different speeds. Seven photoelectric sensors are mounted on the beams to monitor the moving speed of the car. The second sensor is located at the point where the front wheels of the car just get on the main beam, and the last sensor is located at the point where the rear set of wheels just get off the main beam. They are used to measure the speed of the model car.. The others are located on the main beam at a spacing of 0·776 m to check on the uniformity of the speed.

Three strain guages and four accelerators are mounted at the bottom of the main beam to measure the responses. One gauge and one accelerator are mounted at each of the cross-sections at the 1/4, 1/2 and 3/4 spans. The fourth accelerator is mounted at the 3/8 span. An eight-channel dynamic testing and analysis system (DTAS) is used for data collection in the experiment. The first channel is used to monitor the signal of the photoelectric sensors. The second, third and fourth channels are used to measure the signal of the strain gauges. The remaining channels are used to measure the acceleration responses. The sampling frequency is 128 Hz.

The model car has two axles at a spacing of 0·203 m and in runs on four rubber wheels. The mass of the whole car is 7·1 kg. The bouncing, pitching and rolling natural frequencies of the car are 27·5, 42·9 and 69·4 Hz respectively. The first three natural frequencies of the beam are 6·6, 18·5 and 39·5 Hz. The average speed of the car is 3·102 m/s in the present study.

In this practical case when $\mathbf{f}_{true}$ is not known, the seminorm of the solution against the regularization parameter B is plotted. The seminorm of the estimated forces is

$$E1 = \| \mathbf{f}_{j+1}^{(identify)} - \mathbf{f}_{j}^{(identify)} \|, \tag{31}$$

where $\mathbf{f}_{j}^{(identify)}$, $\mathbf{f}_{j+1}^{(identify)}$ are the identified forces with $\mathbf{B}_j$ and $\mathbf{B}_j + \Delta\mathbf{B}$. The value of $\mathbf{B}$ which corresponds to the smallest seminorm is the optimal value.

10.1. EXPERIMENTAL PROCEDURES

Before the actual test on the experimental set-up, signals from the strain gauges were inspected and the zero-shift components were identified. The signals were then calibrated by adding masses at the middle of the main beam. During the calibration, the signals of the strain gauges were found to be not very stable and repeatability was not perfectly satisfactory. It is noted that this will lead to calibration errors in the identified results. The car was placed at the right end of the leading beam, and the DTAS was set in pre-trigger state at channel 1. Power for the motor was turned on, and the car moved on top of the beams. Eight channels of signal were acquired. The uniformity of the speed was checked. If the speed was stable, the above steps were repeated to check whether the properties of the structure and measurement system were changed or not. If no significant change was found, the recorded data were accepted. The zero-shifts in the measured signals were removed, and the signals were calibrated with measured channel sensitivities. The time histories between two measured points of the responses were sub-divided into 10 sub-divisions such that the time difference between two time steps is $7{\cdot}8125 * 10^{-4}$ s. A smaller sampling time interval is important for the accuracy of the iterative computation. The measured acceleration records were integrated to velocity records with an algorithm developed by Petrovski and Naumovski [26] with a low-pass filter at 0·0625 Hz.

10.2. SINGLE-FORCE IDENTIFICATION

Nine combinations of the measured responses at 1/4 and 1/2 spans are used to identify the forces as a single force. Correlation coefficients between the reconstructed responses

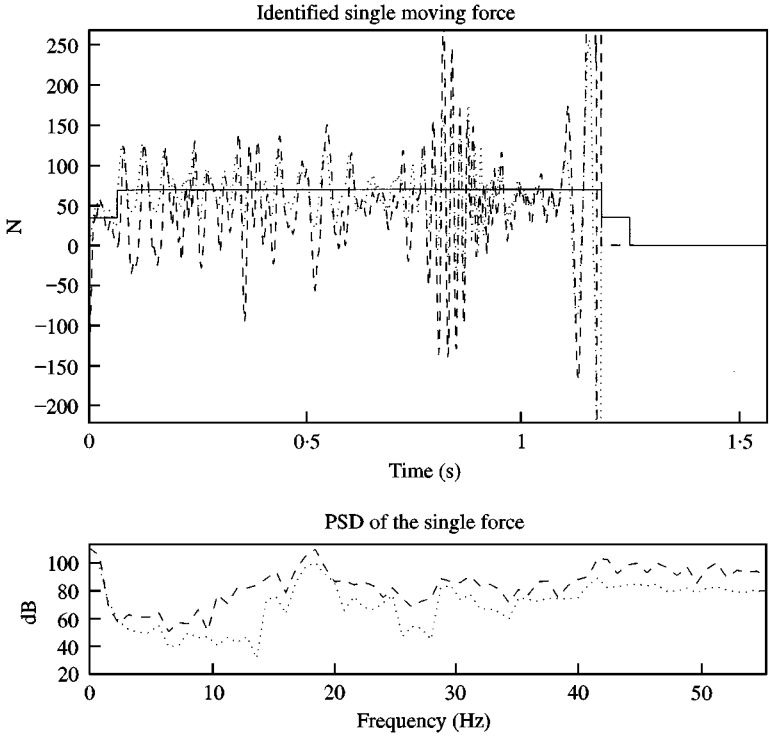

Figure 8. Identified single force and power spectrum from experiment: ——, static force; – – –, 1/4m, 1/2m, ·····, 1/4v, 1/2v.

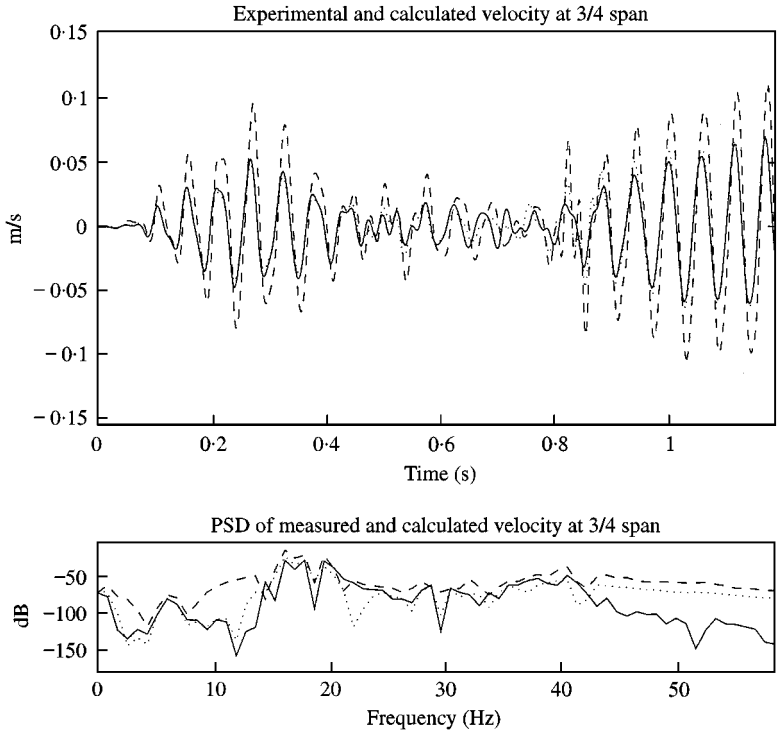

Figure 9. Comparison of velocity at 3/4 span in experiment: ——, measured; – – –, 1/4 m, 1/2m; ·····, 1/4v, 1/2v.

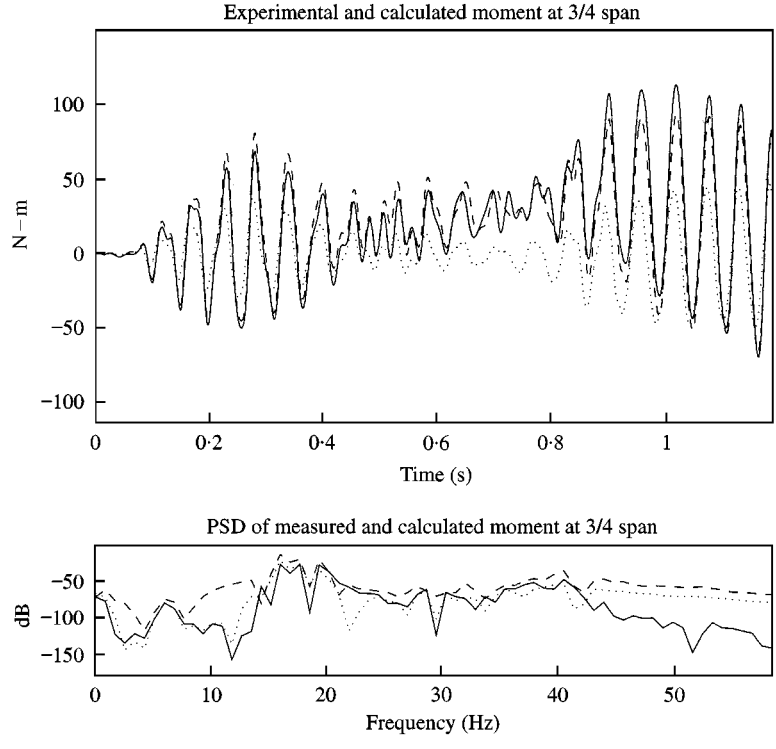

Figure 10. Comparison of bending moment at 3/4 span in experiment: ——, measured; – – –, 1/4 m, 1/2m; ·····, 1/4v, 1/2v.

TABLE 3

Correlation coefficients between measured and reconstructed responses — single-force identification

Combinations of the responses	Comparing moment at 3/4 span	Comparing velocity at 3/4 span
1/2m	0·349	0·155
1/4m	0·801	0·600
1/4v	0·369	0·869
1/2v	0·200	0·254
1/2m, 1/4m	0·939	0·744
1/2v, 1/4v	0·364	0·946
1/4m, 1/2v	0·814	0·629
1/4m, 1/4v	0·796	0·594
1/2m, 1/4v	0·520	0·142

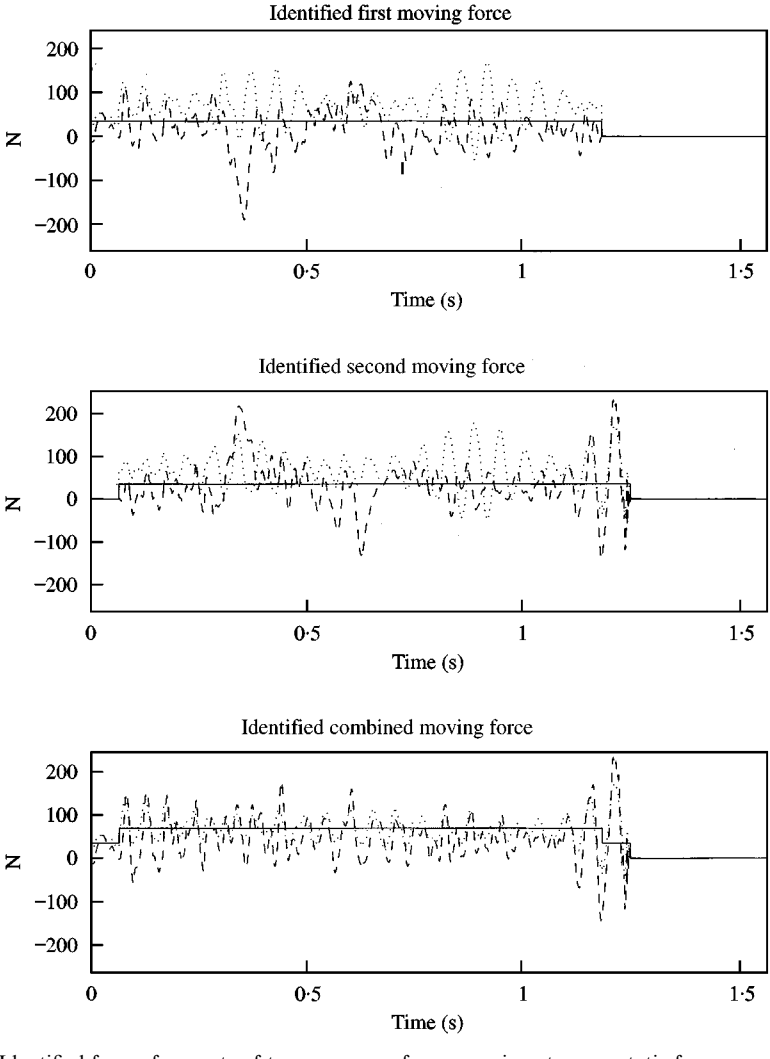

Figure 11. Identified forces from sets of two responses from experiment: ——, static force; – – –, 1/4m, 1/2m, ·····, 1/4v, 1/2v.

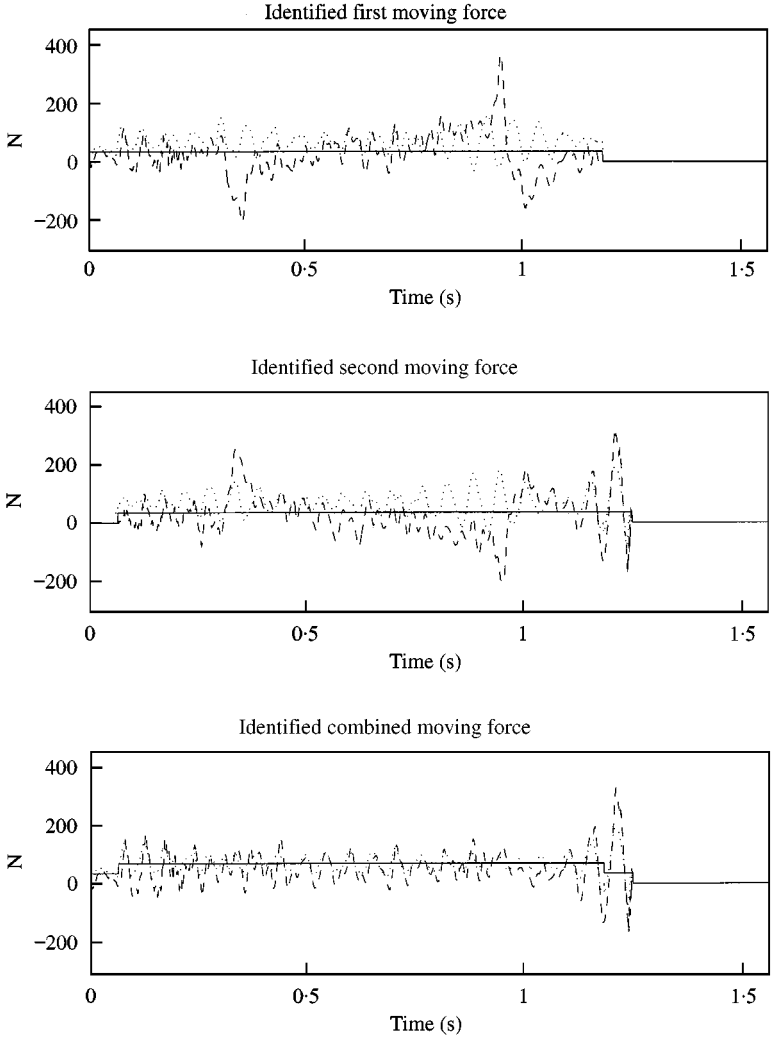

Figure 12. Identified forces from sets of three responses from experiment: ——, static force; – – –, 1/4m, 1/2m, 3/4m; ·····, 1/4v, 1/2v, 3/4v.

using the identified forces and measured responses at 3/4 span are calculated to evaluate the accuracy of the identified force. Clearly, a larger coefficient means that the identified forces are more accurate than that with a smaller coefficient, but the larger coefficient does not mean the identified force is accurate enough because this indirect method of checking on the identified results is not fully sufficient. The coefficients are shown in Table 3, and some of the identified results are shown in Figures 8–10. It is not possible to identify the static component of the forces using only velocity measurements, and the static forces are added to the identified forces in the figures for convenience of comparison.

The results in Table 3 show that the use of bending moments both at 1/2 span and at 1/4 span is most suitable for single moving force identification. Figures 9 and 10 show that the PSDs of the responses match closely, although the time histories are not very close to each other. It is suspected that the calibration errors lead to these differences in the time histories.

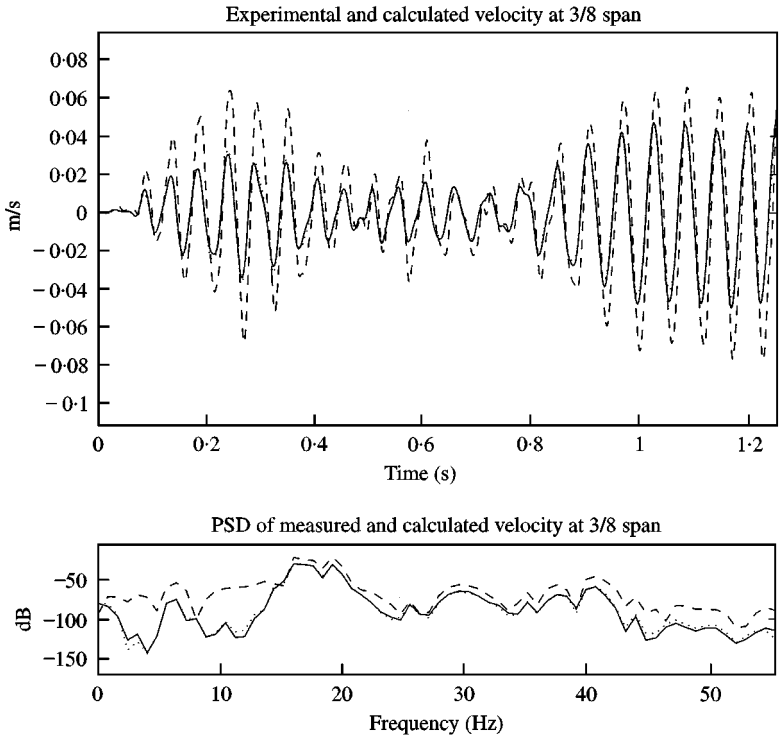

Figure 13. Comparison of velocity at 3/8 span using two responses in experiment: ——, measured; – – –, 1/4m, 1/2m, ·····, 1/4v, 1/2v.

10.3. TWO-FORCES IDENTIFICATION

Twelve combinations of the measured responses are used to identify the two forces separately. The velocity of the main beam at the 3/8 span is reconstructed using the identified forces, and it is compared with the measured response.

Some of the identified results are shown in Figures 11–14. The component with the same amplitude and opposite phase in the two identified forces in Figures 11 and 12 is due to the pitching motion of the model car. The two identified forces are added to obtain a resultant force as shown in the figures. This resulting force can be used as a good estimate of the total equivalent static load of the vehicle.

Figures 13 and 14 show that those curves obtained from using velocity responses closely match the measured responses, while those obtained from using bending moment responses have a large difference in the amplitude. This again leads to the suspicion of the existence of calibration error in the strain measurements.

Correlation coefficients are calculated between the reconstructed and measured responses and they are shown in Table 4. They show that (1) velocity response alone gives better results for the two-forces identification; and (2) 1/4 span responses are better than the other responses. Comparison of the correlation coefficients in Tables 3 and 4 and comparing the responses in Figures 9–12 show that results from the identification as two moving forces are more accurate than those from the identification as a single force.

11. DISCUSSIONS

The ill-conditioned identified forces have large fluctuations in their time histories. Their magnitude are, however, bounded with the use of non-linear least-squares minimization as

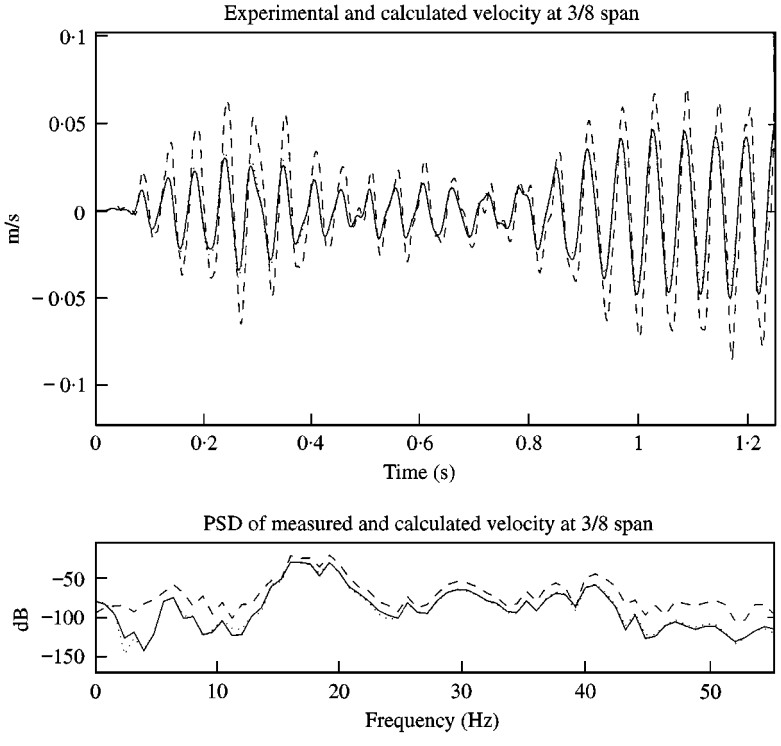

Figure 14. Comparison of velocity at 3/8 span using three responses in experiment: ——, measured; – – –, 1/4m, 1/2m, 3/4; ·····, 1/4v, 1/2v, 3/4v.

TABLE 4

Correlation coefficients between measured and reconstructed velocity at 3/8 *span — two-forces identification*

Response combinations location and type	Correlation coefficient
1/2m, 1/4m	0·742
1/2m, 1/4m, 3/4m	0·748
1/2v, 1/4v	0·989
1/2v, 1/4v, 3/4v	0·988
1/2m, 1/2v	0·018
1/2m, 1/4m, 1/2v	0·743
1/2m, 1/4m, 1/2v, 1/4v	0·744
1/4m, 1/4v	0·739
1/4m, 1/4v, 1/2v	0·747
1/2m, 1/4v	0·236
1/2m, 1/4v, 1/4m	0·743
1/4v, 1/2v, 1/2m	0·245

shown in equation (14), and the errors computed for the identified forces are much smaller than those obtained from TDM [18] without regularization. However, the short periods at the start and end of the time histories still contribute greatly to the total error as computed from equation (30). This error can be reduced as reported by Choi and Chang [27] by using

different smaller **B** matrix at these two time durations. The forces identified from the experimental data are fairly smooth varying around the static force, and the identified combined force can be useful as a reliable estimate of the static weight of the vehicle crossing the bridge.

12. CONCLUSIONS

A method based on dynamic programming is developed to identify moving forces from measured responses of a simply supported beam. This method provides bounds to the identified forces in solving the ill-conditioned problem, and the errors of identification are much smaller than those obtained from the existing time domain method in comparing the identified forces from using different combinations of measured responses in both simulation and laboratory studies. The state-space formulation of the dynamic system can be extended to include a more complicated finite element model of a structure under multi-forces excitation.

ACKNOWLEDGMENTS

The work described in this paper was supported by a grant from the Hong Kong Polytechnic University Research Funding Project No. S571.

REFERENCES

1. R. CANTINENI 1992 *Swiss Federal Laboratories for Materials Testing and Research* (*EMPA*) *Report No*. 220, 240p. Dynamic behaviour of highway bridges under the passage of heavy vehicles.
2. R. J. HEYWOOD 1994 *International Journal of Vehicle Design*. Influence of truck suspensions on the dynamic response of a short span bridge.
3. M. F. GREEN and D. CEBON 1994 *Journal of Sound and Vibration* **170**, 51–78. Dynamic response of highway bridges to heavy vehicle loads: theory and experimental validation.
4. Y. B. YANG and J. D. YAU 1997 *Journal of Structural Engineering*, *ASCE* **123**, 1512–1518. Vehicle–bridge interaction element for dynamic analysis.
5. K. HENCHI, M. FAFARD and G. DHATT 1998 *Journal of Sound and Vibration* **212**, 663–683. An efficient algorithm for dynamic analysis of bridges under moving vehicles using a coupled modal and physical components approach.
6. R. J. PETERS 1984 *Proceedings of* 12*th ARRB Conference*, Vol. 12, 10–18. A system to obtain vehicle axle weights.
7. R. J. PETERS 1986 *Proceedings of* 13*th ARRB and* 5*th REAAA Combined Conference*, Part 6, 70–83. An unmanned and undetectable highway speed vehicle weighing system.
8. G. WHISTON 1984 *Journal of Sound and Vibration* **97**, 35–51. Remote impact analysis by use of propagated acceleration signals, I: theoretical methods.
9. R. JORDAN and G. WHISTON 1984 *Journal of Sound and Vibration* **97**, 53–63. Remote impact analysis of use of propagated acceleration signals, II: comparison between theory and experiment.
10. J. MICHAELS and Y. H. PAO 1986 *Journal of Applied Mechanics* **53**, 61–68. Determination of dynamic forces from wave motion measurements.
11. J. F. DOYLE 1984 *Experimental Mechanics* **24**, 265–270. Further developments in determining the dynamic contact law.
12. J. F. DOYLE 1987 *Experimental Mechanics* **27**, 229–233. An experimental method for determining the location and time of initiation of an unknown dispersing pulse.
13. H. R. BUSBY and D. M. TRUJILLO 1987 *Computers and Structures* **25**, 109–117. Solution of an inverse dynamics problem using an eigenvalue reduction technique.
14. P. E. HOLLANDSWORTH and H. R. BUSBY 1989 *International Journal of Impact Engineering* **8**, 315–322. Impact force identification using the general inverse technique.

15. S. S. SIMONIAN 1981a *International Journal of Numerical Method in Engineering* **17**, 357–365. Inverse problems in structural dynamics—I. Theory.
16. S. S. SIMONIAN 1981b *International Journal of Numerical Method in Engineering* **17**, 367–386. Inverse problems in structural dynamics—II. Applications.
17. J. DRUZ, J. D. CRISP and T. RYALL 1991 *AIAA Journal* **29**, 464–470. Determining a dynamic force on a plate—an inverse problem.
18. S. S. LAW, T. H. T. CHAN and Q. H. ZENG 1997 *Journal of Sound and Vibration* **201**, 1–22. Moving force identification: a time domain method.
19. S. S. LAW, T. H. T. CHAN and Q. H. ZENG 1999 *Journal of Dynamic Systems, Measurement and Control ASME* **12**, 394–401. Moving force identification: a frequency and time domains analysis.
20. T. H. T. CHAN, S. S. LAW, T. H. YUNG and X. R. YUAN 1999 *Journal of Sound and Vibration* **219**, 503–524. An interpretive method for moving force identification.
21. H. R. BUSBY and D. M. TRUJILLO 1993 *Inverse Problems in Engineering: Theory and Practice*. ASME Press, USA, 155–161. An inverse problem for a plate under pulse loading.
22. J. C. SANTANTAMARINA and D. FRATTA 1998 *Introduction to Discrete Signals and Inverse Problems in Civil Engineering*. ASCE Press, USA, 200–238.
23. A. N. TIKHONOV 1963 *Soviet Mathematics* **4**, 1035–1038. On the solution of ill-posed problems and the method of regularization.
24. D. M. TRUJILLO 1978 *International Journal of Numerical Methods in Engineering* **12**, 613–624. Application of dynamic programming to the general inverse problem.
25. R. BELLMAN 1967 *Introduction to the Mathematical Theory of Control Processes*. New York: Academic Press.
26. J. PETROVSKI and N. NAUMOVSKI 1979 *Report* 66. I211S, Stronjze. Processing of strong motion accelerograms. Part 1: analytical methods.
27. K. Y. CHOI and F. K. CHANG 1996 *AIAA Journal* **34**, 136–142. Identification of impact force and location using distributed sensors.

APPENDIX A: NOMENCLATURE

$g_n(X)$	solution corresponds to the nth stage of dynamic programming
l	length of finite beam element
u_1, u_2	finite element end translations
$\mathbf{f}_j$	vector of force in the jth stage of forward process
$\mathbf{u}$	vector of all displacements
$\dot{u}$	first derivative of $\mathbf{u}$ with respect to time
$\mathbf{A}$, $\mathbf{B}$	weighting matrices
$\mathbf{C}$	system damping matrix
E	least-squares error of the solution
$\mathbf{F}$	exponential matrix
$\mathbf{G}$	system matrix
$\mathbf{K}$	system stiffness matrix
$\mathbf{M}$	system mass matrix
R_i, M_i	the ith nodal vertical force and moment
$\mathbf{P}$	global nodal force vector
$\mathbf{Q}$	selection matrix
$\mathbf{R}_n$, $\mathbf{S}_n$	initial conditions in the backward process of dynamic programming
$\mathbf{X}$	vector of state variable of displacement and velocity
$\mathbf{Y}$	matrix of information on force location
$\mathbf{Z}$	measurement vector